OPEN ACCESS

**Nexus Global Research Journal of Engineering And Innovative Technology**
ISSN: XXXX-XXXX(Online)
*Vol-1, Issue-1 (Jun-2026) pp-01-23* Journal Homepage: https://nexusglobalresearch.com/ngrjeit/

Research Article

# 4d Seismic, Ant-Attribute Assisted Interpretation of Induced-Stress Change in Hydrocarbon Producing Reservoir Using Timelapse and Well Log Data.

**Orji, C. Stephen,[1] Iyeneomie Tamunobereton-Ari,[2] A. R. C. Amakiri,[3] Jiriwari Amonieah[4]**

*[1-4]Department of Physics, Rivers State University, PMB 5080, Port Harcourt, Rivers State, Nigeria.*

**ABSTRACT:**
The changes in reservoir pore pressure due to hydrocarbon production induces stress changes within the reservoir and its surrounding rocks. These stress changes lead to reservoir compaction, which in turn can trigger potential geomechanical problems such as surface subsidence, fault reactivation, wellbore instability, pore collapse, casing deformation and seismicity. In this study, we present a 4D seismic, ant-attribute assisted, interpretation of induced-stress change in hydrocarbon producing reservoir in Kolo-Creek Field, Coastal Swamp Niger Delta, Nigeria. The analysis integrates 3D seismic interpretation, ant-attribute evaluation, well-log analysis, pressure and production data. Time-lapse seismic surveys acquired in 1997 (base) and 2009 (monitor) show clear 4D responses with a root-mean-square repeatability ratio (RRR) of 0.38, indicating excellent survey repeatability. The seismic interpretation reveals fault reactivation and fracturing associated with production-induced stress changes. Geophysical well logs from seven wells were used to delineate and correlate three reservoir zones (Sand A, Sand B, and Sand C). Petrophysical analysis indicates low shale content ranging from 7.74–37.44%, high porosity values between 0.19 and 0.36), and excellent permeability varying from 375–3327 mD, which is consistent with high-quality, coarse-grained sandstones. Production and pressure data provided by SPDC show a decline from 1592.55 to 400.34 bbl/day and from 4766 to 3103 psi over 12 years, respectively, corroborating with the ant-tracker attribute interpretation. Variance attribute was used to delineate faults and the result obtained from variance attribute were used as an input in running the Ant tracker attributes to delineate subtle faults in both base and monitor that are difficult to see easily. The results obtained from the ant attribute monitor volume indicate that the subtle faults seen in the base volume are fractured, reactivated in the monitor causing reduction in the porosity of the reservoir and in turn resulting to reservoir compaction and subsidence. The integration of ant tracker attribute with structural analysis reveals reservoir stress changes on fault behavior and reservoir performance. This study could lead to Wellbore Stability Management; Using stress change predictions to guide well placement and drilling orientation, minimizing risks of shear failure, casing deformation, and production losses.

***Keywords:*** *Seismic attributes, induced-stress, Ant trackers attributes, 3D seismic cubes, structural mapping, faults and fractures Nigeria.*

## 1. INTRODUCTION

The production of hydrocarbon is associated with the deformation and displacement of reservoir rock properties both inside and outside the reservoir. This deformation induces-stress change in the rock properties inside the reservoir due to fluid production and this process could lead to fault re-activation, fractures, pore pressure depletion, loss of porosity and permeabilities, which result to compaction as overburden pressure increases. 4D seismic time-lapse is a method used in evaluating induced stress change in a reservoir. Seismic attributes provide a quick way to visualize the signal to map out discontinuities, subtle variation, detection of anomalies caused by faults and fractures and also the trends of faults which are hard to see on a conventional 3D data set. Ant tracker attributes analysis was carried out to evaluate the induced stress change in a producing reservoir in Niger Delta. Although, several attributes enhance clarity of faults on seismic data such as variance attributes, ant attributes, chaos attributes, curvature attributes etc. among all, ant attributes show better result in delineating faults. The effective implementation of

**Corresponding author:** A. R. C. Amakiri, Email: amakiri.arobo@ust.edu.ng
**Received:** 25 May 2026; **Accepted:** 01 June 2026; **Published:** 06 June 2026
Copyright © 2026 The Author(s): This work is licensed under a Creative Commons Attribution- Non-Commercial-No Derivatives 4.0 (CC BY-NC-ND 4.0) International License

ant tracker attribute is achieved by using the output of other fault sensitive attributes as an input data. In this work, the seismic data used was carefully conditioned using structural smoothing to remove residual background noise and to improve the spatial continuity of seismic signal as seen in Figures 13 - 15. Then, variance attributes which is sensitive to faults is applied to the seismic data set; and the outputs from these processes is used as our input data to run the ant attribute with which the subtle faults were clearly seen that were difficult to display on the raw seismic data set. In this study, well logs data, seismic data, pressure and production data were analyzed and interpreted in order to evaluate stress changes in a producing reservoir in Kolo-Creek Field, Nigeria. The results obtained from the ant attribute monitor volume indicate that the subtle faults seen in the base volume are fractured, reactivated in the monitor volume causing reduction in the porosity and permeability of the reservoir, leading to pressure depletion and change in stress and strain in the overburden reservoir.

## 2. LOCATION AND GEOLOGY OF THE STUDY AREA

The Kolo-Field OML-28 Field is the study area and it is located in the Northeast of Bayelsa State and lies on latitudes 4º50'58''-4º55'19''N and longitudes 6º18'41''-6º26'41''E (Figure 1). The Kolo-Field is located in the Coastal Swamp Depobelt Niger Delta of aerial extent of about 840 km$^2$. The main reservoir is oil bearing, located at a depth range of 3580-3670m with thickness of about 50-60m with a sedimentary sequence described as mainly a deltaic depositional sub-environment. The Kolo-Field Reservoir, characterized by numerous predominantly E trending growth faults, is of the Middle Miocene and of the Agbada Formation (Oboh, 1993). Kolo-Field is made up of fresh water and marine swamps with relief increasing Northwards (Uko *et al*., 1992). Like other deltaic regions in the world, it is characterized by both marine and mixed continental depositional environment.


**Figure 1: Location of The Study Area in A Yellow Box (After Ejedawe *Et Al.*, 2007).**

## 3. MATERIALS AND METHODS

The data consist of base and monitor seismic data acquired at different Vintages, suite of well logs which include: velocity logs (Vp and Vs), Gamma ray log, density log, neutron log, resistivity log, caliper log, well information (i.e. well header, deviation data, well tops, derrick floor elevation and well check shots data, production and pressure data from seven wells (Well A, B, C, D, E, F and G). However, due to the gaps and null values in some wells, not all were used in the analysis. These data were analysed using Schlumberger-owned interpretation and visualization software Petrel 2016.3 edition, 3DFieldPro software was used for overburden velocity analysis, contouring and ant tracker attributes analysis. For rock physics-based reservoir characterization, Hampson Russell Software Version 10.4.2 owned by CGG GeoSoftware was used. The methodology to estimate quantitative petrophysical properties from

wireline log data using various rock physics models has the following stages: Well log preparation and editing, delineation of reservoir beds and well log correlation, petrophysical properties estimation, carried out well-to-seismic tie; generate the difference cube from the base and monitor data and quantify the repeatability (RRR) for the time-lapse seismic data and estimation of ant tracker attribute.

### 3.1 Delineation of Reservoir Beds

This is the process of determining reservoir zones with considerable hydrocarbon saturation. Logs respond to different lithologies. The gamma ray (GR) log is particularly useful for defining shale beds as well as the Spontaneous Potential (SP) log. The GR log reflects the proportion of shale and, in many regions, can be used quantitatively as a shale indicator.

### 3.2 Litho-stratigraphy correlation

A horizon represents an isochronous geologic time surface. It is the interface between two different rocks layers. It is associated with continuous and reliable reflection on the sections that appear over a large area. In order to perform a log analysis, it is necessary to pick the various zones of interest. In this study, selection of values was made on a consistent basis from day to day to assist reproducibility of results.

### 3.3 Computation of Petrophysical Properties

#### 3.3.1 Volume of shale (Vsh)

Dresser proposed a new approach as a result of empirical correlation where the relationship changes according to the age or volume content of the formation. Younger rocks (Tertiary), unconsolidated.

$$V_{sh} = 0.083\ (2^{3.7\ IGR} - 1) \quad (1)$$

where $I_{GR}$ = Gamma ray index

$V_{sh}$ = shale volume

The gamma-ray index can be obtained from the linear equation:

$$I_{GR} = \frac{GR_{\log} - GR_{\min}}{GR_{\max} - GR_{\min}} \quad (2)$$

where $I_{GR}$ = Gamma Ray Index; $GR_{\log}$ = Gamma Ray Reading from Log; $GR_{\min}$ = Minimum Reading of Gamma Ray Log; $GR_{\max}$ = Maximum Gamma Ray Reading

#### 3.3.2 Determination of Water Saturation (Sw)

Water Saturation is mathematically expressed as:

$$S_w = \left( \frac{a \times R_w}{\Phi^m R_t} \right)^{1/n} \quad (3)$$

where Sw = Water saturation; a = Tortuosity factor; m = Cementation factor; n = Saturation exponent; Φ = Porosity of the formation; Rt = Deep resistivity of the formation.

#### 3.3.3 Total Porosity (Φt) and Effective Porosity (Φeff)

In this work, the density log was used for the determination of the porosity by applying the equation [5]. Total Porosity was calculated from density porosity log using the equation:

$$\Phi_T = \frac{\rho_{ma} - \rho_b}{\rho_{ma} - \rho_f} \quad (4)$$

$$\Phi_{eff} = \Phi_T - \left( \Phi_{sh} \times V_{sh} \right) \quad (5)$$

Where, $\Phi_T$ = Total Porosity; $\rho_{ma}$ = Density of the rock matrix; $\rho_b$ = Bulk density read directly from the log; $\rho_f$ = Fluid density; $\Phi_{eff}$ = Effective Porosity; $\Phi_{sh}$ = Total Porosity of Shale; $V_{sh}$ = Volume of shale.

**3.3.4 Determination of Net/Gross Reservoir Thickness**

The net reservoir thickness was obtained for all the reservoirs in the wells.

$$\mathrm{h} = \mathrm{H} - h_{\mathrm{shale}} \quad (6)$$

$$\mathrm{Net/Gross} = \mathrm{h/H} \quad (7)$$

Where: H = gross reservoir thickness; h= net reservoir thickness, $h_{\mathrm{shale}}$= shale thickness

**3.3.5 Determination of Permeability (K)**

The permeability values for the observed reservoirs were calculated using the equation after method [3].

$$K = \left[\frac{250 \times \Phi^3}{S_{wirr}}\right]^2 \quad (8)$$

$$S_{wirr} = \sqrt{\frac{F}{2000}} \quad (9)$$

$$F = \frac{0.81}{\Phi^2} \quad (10)$$

where $S_{wirr}$ = Irreducible Water Saturation; $F$ = Formation Factor; $\Phi$ = Porosity; K= Permeability

**3.4 Seismic Intepretation**

**3.4.1 Well Log Conditioning**

Sonic logs were adjusted according to seismic measurements in the boreholes because sonic times obtained through the integration of sonic logs usually differ from those obtained using a well seismic. The reasons for drift range from basic discrepancies between two approaches due to different geometry/frequency of measurement principles. Therefore, it is necessary to calibrate the sonic logs to eliminate these possible errors to use it for seismic applications for a particular area.

**3.4.2 Checkshot**

The checkshot survey provides accurate depth-time relationship between the seismic data and well log data. This is essential for calibrating seismic data to obtain the true subsurface depths, thereby enhancing the accuracy of reservoir characterization

**3.4.3 Well-to-Seismic tie**

This relates subsurface measurements obtained at a wellbore measured in depth and seismic data measured in time. It provides a means of correctly identifying horizons to pick and interprete the seismic data in terms of geological structure and properties

**3.4.4 Horizon Interpretation**

The horizons were picked based on stratigraphic information and formation tops provided by wells in the study region immediately after the seismic-to-well tie process. The subsurface structure was interpreted seismically by selecting horizons along coherent reflections of the same phase and it is shown in Figure 6. Horizon (Sand D-2) was interpreted on every 10-inline or cross-lines interval. Interpreted horizons are representative of the Niger Delta anticlinal structures with E-W trending synthetic and antithetic faults.

**3.4.5 Time Surface Generation**

The seed grids for the three horizons that were digitized were used as the input for generating the reservoir time structure surfaces. Before generating the surfaces, the fault traces on the seeded grids were mapped as polygons which are a basic requirement for building a reservoir structural model. The seed grids were then converted to surfaces using convergent interpolation algorithm.

**3.4.6 Depth Surface Generation**

Depth surfaces were generated after the TDR function was run on the time surfaces. For a depth conversion to be considered good, the depth surfaces should show no significant differences in structure with the equivalent time structure surfaces. After depth conversion, the top structure maps that have been depth converted were used to generate the base structure map through an interpolation process called surface re-adjustment.

**3.4.7 Velocity Modelling**

Time Depth Relationship (TDR) function was utilized for converting the surfaces from time to depth.

The third order polynomial function gave the best fit to the velocity data and hence was used as the input for the velocity model conversion. The equation was utilized in Petrel calculator for the conversion of surfaces from time to depth. This is shown in Figure 10

Equation below defines this model:

$$\boldsymbol{V}(z) = \boldsymbol{V}_0 (\boldsymbol{z} + \boldsymbol{KZ}). \quad (11)$$

Where, V(z) is the instantaneous velocity, Z is depth, Vo(m/s) is the top-interface velocity, and K(s1) is the velocity gradient or compaction factor.

**3.4.8 Seismic Attribute Analysis**

Variance attributes were used to map the structure and shape of geological features of interest, such as faults, subtle faults, anticlines, channels and fractures. This is shown in Figure 9

**3.4.9 Fault Interpretation.**

The variance coherency property was utilized to aid in the depiction of faults that were difficult to identify in the original seismic data as shown in Figure 10.

**3.4.10 Structural Smoothing:**

Structural smoothing was carried out on the seismic data to enhance the visibility of geological structures and reduced noise. This is shown in Figure 13 – Figure 15

**3.4.11 Ant-Tracker Attributes**

The variance attributes which is sensitive to faults is applied to the seismic data set; and the outputs from these processes is used as our input data to run the ant attribute with which the faults were clearly seen that were difficult to display on the raw seismic data set.

**3.5 Determination of Acoustic Impedance from Monitor Seismic Data**

It was used to predict rock properties, such as porosity and fluid saturation. The changes in acoustic impedance were used to indicate changes in rock properties or lithology.

It is calculated using the equation:

$$\mathbf{Z = \rho \times V} \quad \mathbf{(12)}$$

where: ρ = density of the rock; V = velocity of the seismic wave

**3.6 Determination of Effective Pressure**

Eaton's method was used to predict pore pressure in this work. The form of the Eaton equation is

$$P_p = S_v - (S_v - P_n)\left(\frac{A_{obs}}{A_{norm}}\right)^n \quad (12)$$

Where $P_p$ is the pore pressure; $S_v$ is the total vertical stress (overburden or lithostatic pressure); $P_n$ is the normal or hydrostatic pressure; $A_{obs}$ is the observed attribute (sonic travel time, resistivity etc); $A_{norm}$ is the attribute when pore pressure is normal, and n is an empirical constant.

**3.7 Production and Pressure Data**

The Production data which includes; fluid production flow rates of individual wells, cumulative production of each fluid produced from the reservoir over time, gas-oil ratio, water cut and reservoir pressure versus oil days of production of Well C and Well D were obtained from Shell Petroleum Development Company (SPDC), Port Harcourt, Rivers State.

## 4. RESULTS AND DISCUSSION

**4.1 Delineated and Identified Reservoirs**

The delineated reservoirs across the wells of the field showing names, Tops, Bases, and thicknesses is presented in Table 4.1. Three reservoirs (Sand 1, 2 and 3) were delineated for each of the seven wells. The thickness of the wells varied from 43-245 ft and the wells display a sand-shale intercalated sequence, which is characteristic of the Niger delta formation. Shale lithologies were defined by high gamma ray values. Regions showing low gamma ray, and high resistivity are mapped as sand lithologies and these are considered reservoirs.

**Table 1: Reservoir Delineation of the Field Showing Name, Top Depth, Base Depth and thickness**

| Well | Reservoir Name | Top MD (Ft) | Base MD (Ft) | Thickness (Ft) |
|---|---|---|---|---|
| Well A | *Sand 1* | 6869 | 6930 | 61 |
| | *Sand 2* | 10477 | 10593 | 116 |
| | *Sand 3* | 11508 | 11731 | 223 |
| Well B | *Sand 1* | 7188 | 7239 | 51 |
| | *Sand 2* | 10790 | 10907 | 117 |
| | *Sand 3* | 11780 | 11975 | 195 |
| Well C | *Sand 1* | 7015 | 7075 | 60 |
| | *Sand 2* | 10926 | 11032 | 106 |
| | *Sand 3* | 11946 | 12191 | 245 |
| Well D | *Sand 1* | 6925 | 6970 | 45 |
| | *Sand 2* | 10879 | 10984 | 105 |
| | *Sand 3* | 12010 | 12247 | 237 |
| Well E | *Sand 1* | 7105 | 7162 | 57 |
| | *Sand 2* | 10723 | 10867 | 144 |
| | *Sand 3* | 11755 | 11963 | 208 |
| Well F | *Sand 1* | 7039 | 7082 | 43 |
| | *Sand 2* | 10890 | 10945 | 55 |
| | *Sand 3* | 11935 | 12099 | 164 |
| Well G | *Sand 1* | 6941 | 6984 | 43 |
| | *Sand 2* | 10621 | 10728 | 107 |
| | *Sand 3* | 11726 | 11915 | 189 |

### 4.2 Lithologic Correlation

Lithologic units were identified on the logs and correlated across the wells (Figure 2). The stratigraphic cross-sections produced show a general lateral continuity of the lithologic units across the field. Three zones of interest (Sand 1, Sand 2 and Sand 3) were delineated and correlated across all seven wells. The litho-stratigraphy correlation section revealed that each of the sand units' spreads over the field and differs in thickness with some units occurring at greater depth than their adjacent unit.

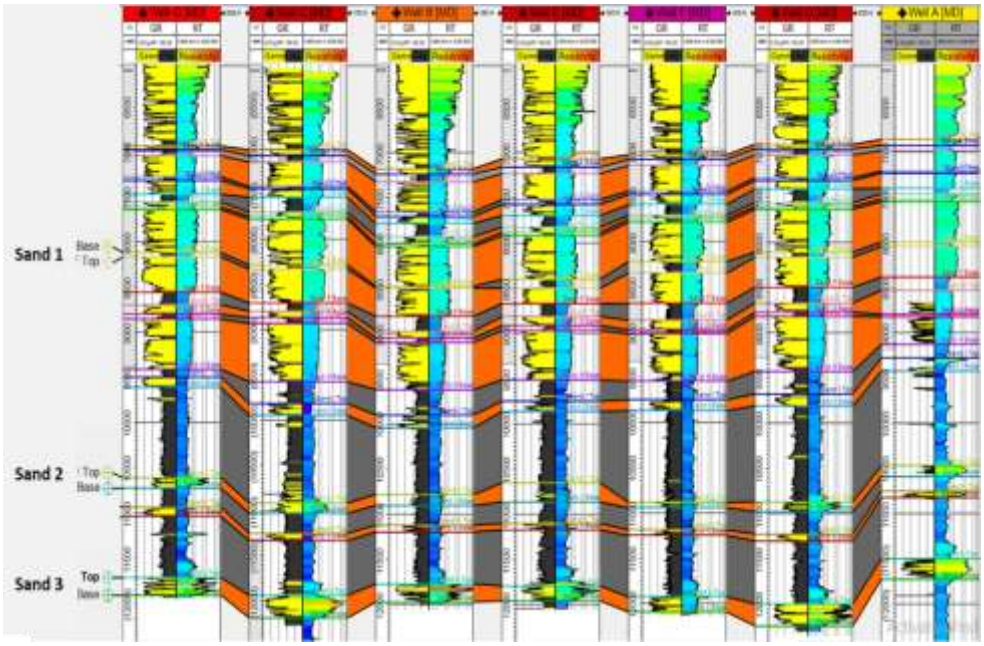


**Figure 2: Well log Section Showing the Reservoirs Delineated and Correlated across Seven Wells**

**4.3 Petrophysical Properties Evaluation**

The estimated values of the several petrophysical parameters, using the appropriate empirical models stated previously, are presented in Tables 2 - 5. The wells are Well A, Well B, Well C, Well D, Well E, Well F and Well G. After the wells were delineated, petrophysical properties were evaluated for each reservoir. The results obtained for the entire reservoirs are thus analysed. The volume of shale was calculated from gamma ray index and the values range from 7.74% to 37.44% indicating that the fraction of shale in the reservoirs is quite low and the volume of sand deposit is larger than shale, therefore, hydrocarbon saturated. These reservoirs are good reservoir with high oil saturation at irreducible water saturation, because volume of shale values is low from 7.74% to 37.44%, which means that the sand body in all the reservoirs is high and there will be high rate of free flow of hydrocarbon in all the reservoirs as corroborated by their permeability values. The total porosity of the reservoirs was estimated from density log (RHOB) using porosity formula and these values ranges from 0.19 to 0.36 indicating a very good reservoir quality and reflecting probably well sorted coarse-grained sandstone reservoirs with minimal cementation. The permeability of the reservoirs ranges from 375 Md to 3327 Md. This implies that the permeability varies from very good to excellent and suggests that these are good (exploitable) reservoir horizon. For a rock to be considered as an exploitable hydrocarbon reservoir without stimulation, its permeability must be greater than approximately 100 md (however, depending on the nature of the hydrocarbon - gas reservoirs with lower permeabilities are still exploitable because of the lower viscosity of gas with respect to oil). This is as a result of very good to excellent sand quality.

**Table 2: Petrophysical Evaluation for Reservoir SAND 1 Reservoir Correlated across Well A to Well G**

| | | Well A | | Well B | | Well C | | Well D | | Well E | | Well F | | Well G | |
|---|---|---|---|---|---|---|---|---|---|---|---|---|---|---|---|
| Petrophysical parameters | Unit | Top 6869 | Base 6930 | Top 7188 | Base 7239 | Top 7015 | Base 7075 | Top 6925 | Base 6970 | Top 7105 | Base 7162 | Top 7039 | Base 7082 | Top 6941 | Base 6984 |
| Gross Thickness | Ft | 61.00 | | 51.00 | | 60.00 | | 45.00 | | 57.00 | | 43.00 | | 43.00 | |
| Shale Volume | % | n.a. | | 10.00 | | 7.74 | | 11.29 | | 18.57 | | 16.29 | | 13.82 | |
| Net Thickness | Ft | n.a. | | 51.30 | | 60.92 | | 45.24 | | 51.35 | | 41.01 | | 42.24 | |
| Net to Gross | | n.a. | | 0.90 | | 0.92 | | 0.89 | | 0.82 | | 0.84 | | 0.86 | |
| Total Porosity | % | 22.37 | | n.a. | | 19.77 | | n.a. | | 32.84 | | 26.74 | | n.a. | |
| Effective Porosity | % | n.a. | | n.a. | | 17.92 | | n.a. | | 25.99 | | 22.12 | | n.a. | |
| Water Saturation | % | 27.98 | | 37.20 | | 34.76 | | 30.34 | | 47.26 | | 33.82 | | 38.17 | |
| Hydrocarbon Saturation | % | 72.02 | | 62.80 | | 65.24 | | 69.66 | | 52.74 | | 66.18 | | 61.83 | |
| Permeability | mD | n.a. | | n.a. | | 1265.53 | | n.a. | | 2171.86 | | 1693.71 | | n.a. | |

**Table 3 Petrophysical Evaluation for Reservoir SAND 2 Reservoir Correlated across Well A to Well G**

| | | Well A | | Well B | | Well C | | Well D | | Well E | | Well F | | Well G | |
|---|---|---|---|---|---|---|---|---|---|---|---|---|---|---|---|
| Petrophysical parameters | Unit | Top 10465 | Base 10587 | Top 10778 | Base 10901 | Top 10914 | Base 11026 | Top 10867 | Base 10978 | Top 10711 | Base 10861 | Top 10878 | Base 10939 | Top 10609 | Base 10722 |
| Gross Thickness | Ft | 122.00 | | 123.00 | | 112.00 | | 111.00 | | 150.00 | | 61.00 | | 113.00 | |
| Shale Volume | % | 28.30 | | 25.04 | | 17.61 | | 24.73 | | 39.09 | | 28.18 | | 22.29 | |
| Net Thickness | Ft | 87.47 | | 92.25 | | 92.29 | | 83.58 | | 91.50 | | 43.81 | | 87.81 | |
| Net to Gross | | 0.72 | | 0.75 | | 0.82 | | 0.75 | | 0.61 | | 0.72 | | 0.78 | |
| Total Porosity | % | 25.20 | | n.a. | | 30.49 | | 26.91 | | 24.57 | | 21.34 | | 28.96 | |
| Effective Porosity | % | 3.00 | | n.a. | | 25.19 | | 20.45 | | 15.04 | | 15.75 | | 22.56 | |
| Water Saturation | % | 18.47 | | 75.56 | | 36.92 | | 23.83 | | 76.84 | | 81.99 | | 33.85 | |
| Hydrocarbon Saturation | % | 81.53 | | 26.44 | | 63.08 | | 76.17 | | 23.16 | | 18.01 | | 66.15 | |
| Permeability | mD | 375.21 | | n.a. | | 2108.74 | | 1454.11 | | 928.88 | | 1036.32 | | 1688.62 | |

**Table 4: Petrophysical Evaluation for Reservoir SAND 3 Reservoir Correlated across Well A to Well G**

| | | Well A | | Well B | | Well C | | Well D | | Well E | | Well F | | Well G | |
|---|---|---|---|---|---|---|---|---|---|---|---|---|---|---|---|
| Petrophysical parameters | Unit | Top 11496 | Base 11725 | Top 11768 | Base 11969 | Top 11934 | Base 12185 | Top 11998 | Base 12241 | Top 11743 | Base 11957 | Top 11923 | Base 12093 | Top 11714 | Base 11909 |
| Gross Thickness | Ft | 229.00 | | 201.00 | | 251.00 | | 243.00 | | 214.00 | | 170.00 | | 195.00 | |
| Shale Volume | % | 37.44 | | 33.13 | | 11.28 | | 13.02 | | 22.50 | | 14.36 | | 20.03 | |
| Net Thickness | Ft | 143.26 | | 134.41 | | 222.69 | | 211.41 | | 165.85 | | 145.59 | | 156.00 | |
| Net to Gross | | 0.63 | | 0.67 | | 0.89 | | 0.87 | | 0.78 | | 0.86 | | 0.80 | |
| Total Porosity | % | 21.00 | | 20.13 | | 29.32 | | 36.86 | | 24.14 | | 20.66 | | 22.58 | |
| Effective Porosity | % | 12.84 | | 14.29 | | 26.44 | | 32.68 | | 19.15 | | 17.97 | | 18.78 | |
| Water Saturation | % | 12.91 | | 22.49 | | 18.99 | | 16.73 | | 22.34 | | 54.10 | | 22.29 | |
| Hydrocarbon Saturation | % | 87.09 | | 77.51 | | 81.01 | | 83.27 | | 77.66 | | 45.90 | | 77.71 | |
| Permeability | mD | 934.80 | | 1005.07 | | 2399.57 | | 3327.39 | | 1365.09 | | 1215.87 | | 1369.88 | |

**Table 5: Summary of Petrophysical Properties for Reservoirs 1, 2 and 3**

| Reservoir Sand | Net Sand Thickness (ft) | | Total Porosity (%) | | Effective Porosity (%) | | Water Saturation ($S_w$) (%) | | Permeability (mD) | |
|---|---|---|---|---|---|---|---|---|---|---|
| | Range (ft) | Average (ft) | Range (%) | Average (%) | Range (%) | Average( %) | Range (%) | Average (%) | Range (mD) | Average (mD) |
| 1 | 6869-7188 | 51.4 | 19.77-32.84 | 24.3 | 17.92-25.99 | 22.01 | 27.98-38.17 | 35.60 | 1265.53-2171.86 | 1710.4 |
| 2 | 10465-11026 | 113.1 | 21.34-30.49 | 26.2 | 3.00-25.19 | 17.00 | 18.49-81.99 | 49.40 | 375.21-2108.74 | 1265.3 |
| 3 | 11494-12241 | 214.7 | 21.00-36.86 | 25.00 | 12.84 - 26.44 | 20.3 | 45.90-87.09 | 24.30 | 934.80-3327.39 | 1656.7 |
| Average | | 126.4 | | 25.20 | | 19.8 | | 36.40 | | 1544.1 |

### 4.4 Seismic Intepretation

#### 4.4.1 Well Log Conditioning

Sonic logs were adjusted to suit the seismic measurements in the boreholes. This is because the sonic times obtained from sonic logs are usually differ from those obtained using a well seismic. Therefore, it is necessary to calibrate the sonic logs to eliminate these possible errors before using it for seismic applications This was done on well A as shown in Figure 3

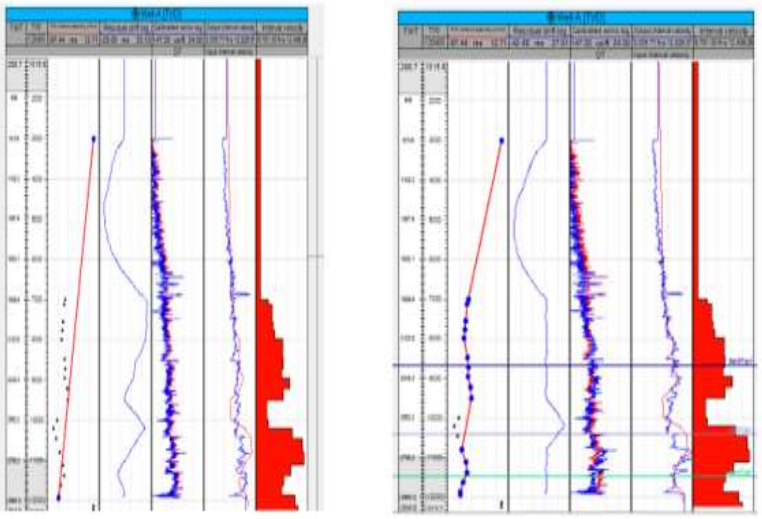

**(a)** **(b)**

**Figure 3: (a) Drift Analysis before sonic log calibration done on Well A. (b) Drift Analysis after sonic log calibration done on Well A**

#### 4.4.2 checkshot

The checkshot, sonic and density logs for the well were first checked for unit consistencies and missing intervals.

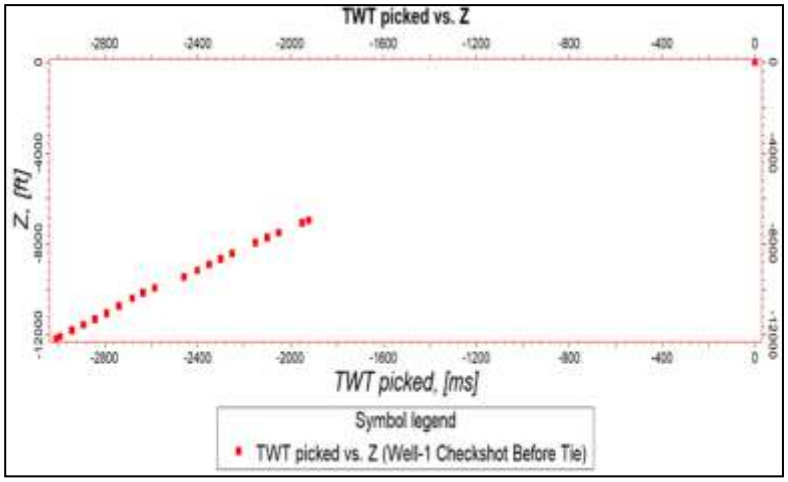


**Figure 4: Quality of Well-E Checkshot Utilized for Well-to-Seismic Tie**

**4.4.3 Seismic-to-Well Tie**

Well-to-seismic tie was carried out using synthetic seismograms generated along well E that have checkshots and complete sonic and density logs shown in Figure 4. This process manually stretches or squeezes the log in order to improve the time correlation between the target log and the seismic attributes as shown in Figure 5b

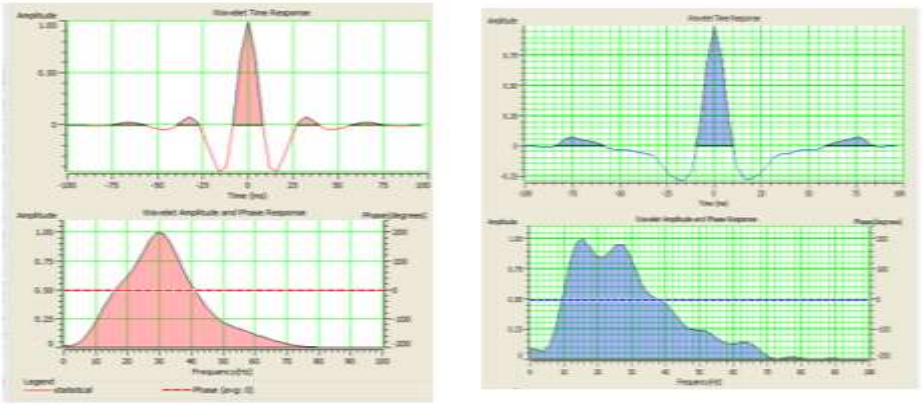

**Figure 5: (a) Extracted Wavelet from Well A with Average Phase (-2), and Frequency Content of 5Hz. This replaces the Lost in low Frequency content in Seismic Data.**

**(b) Extracted Wavelet for Seismic to Well Tie with Average Phase (0), with Frequency Content of 75Hz**

**4.4.4 Horizon Interpretation**

The horizons were picked based on stratigraphic information and formation tops provided by wells in the study region. Horizon (Sand D-2) was interpreted on every 10-inline or cross-lines interval. The interpreted horizons show the Niger Delta anticlinal structures with E-W trending synthetic and antithetic faults.

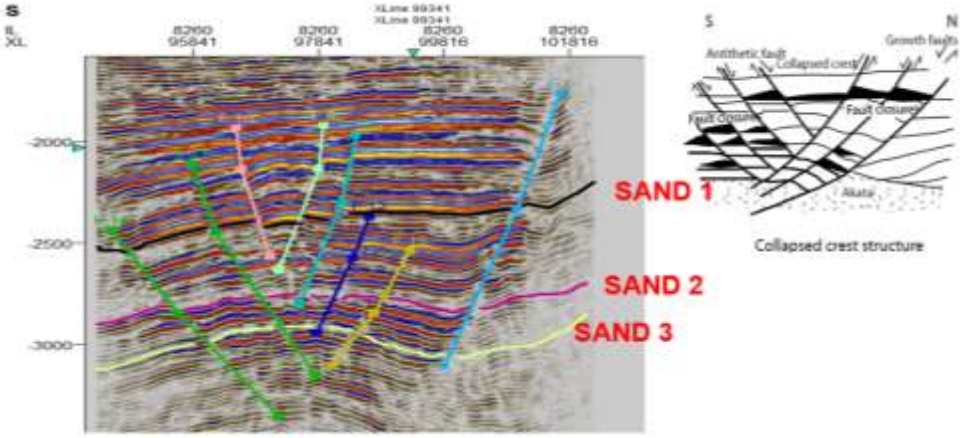


**Figure 6: Seismic inline 8260 showing interpreted synthetic and antithetic faults and Horizons (Inset figure on common fault types in Niger Delta, After Doust and Omatsola, 1990)**

### 4.4.5 Time Surface Generation

The seed grids for the three horizons that were digitized were used as the input for generating the reservoir time structure surfaces. Before generating the surfaces, the fault traces on the seeded grids were mapped as polygons which are ~~a~~ basic requirement for building a reservoir structural model.

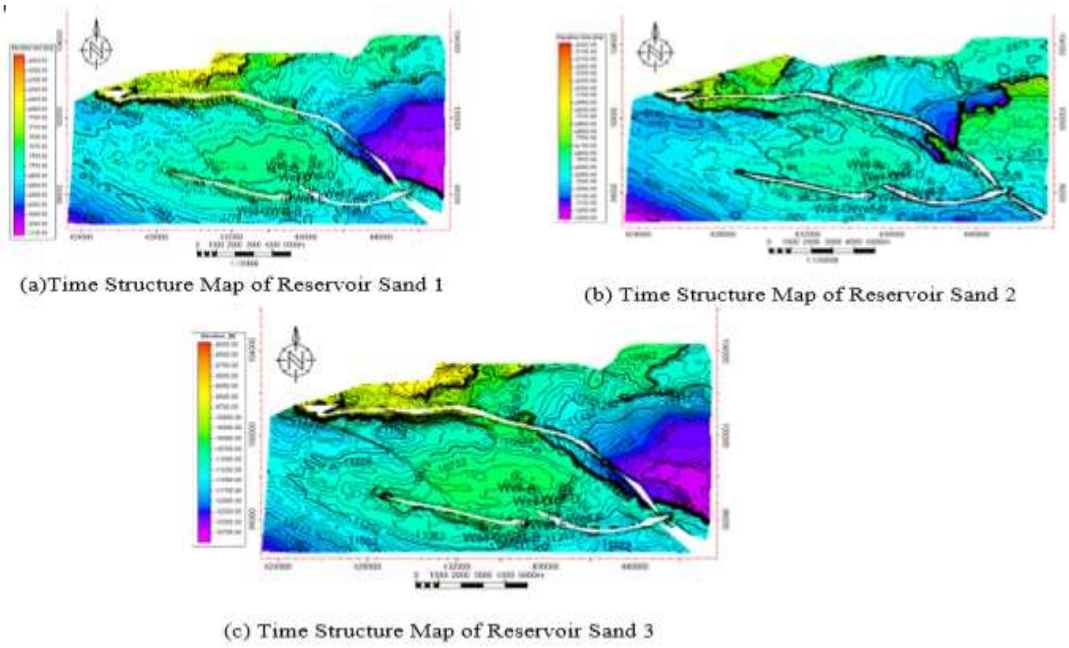


**Figure 7: Time Structure Map of Reservoir Sands**

### 4.4.6 Depth Surface Generation

Depth surfaces were generated after the TDR function was run on the time surfaces. After depth conversion, the top structure maps that have been depth converted were used to generate the base structure map through an interpolation process called surface re-adjustment.

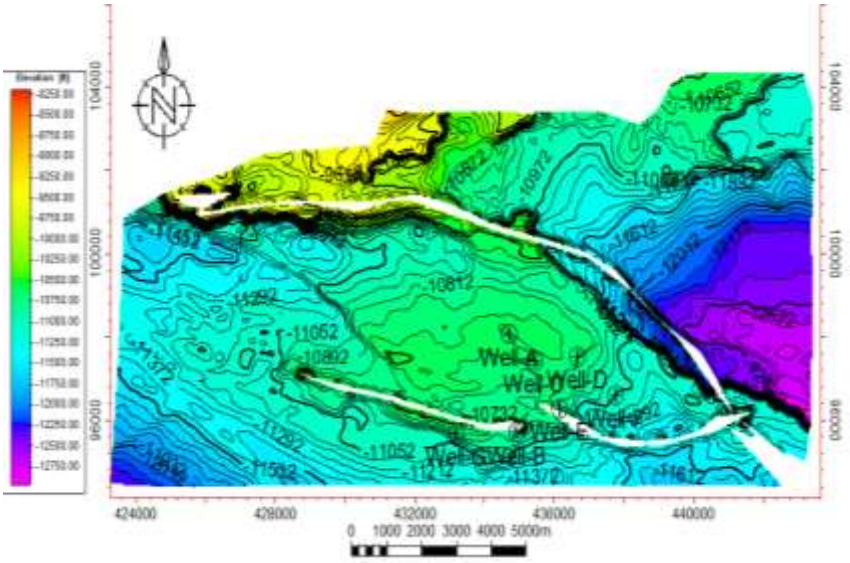


**Figure 8**: **Depth Map of Reservoir Sand 1**

### 4.4.7 Velocity Modelling

Time Depth Relationship (TDR) function was utilized for converting the surfaces from time to depth. The third order polynomial function gave the best fit to the velocity data and hence was used as the input for the velocity model conversion. The equation was utilized in Petrel calculator for the conversion of surfaces from time to depth. This is shown in Figure 10

Equation below defines this model:

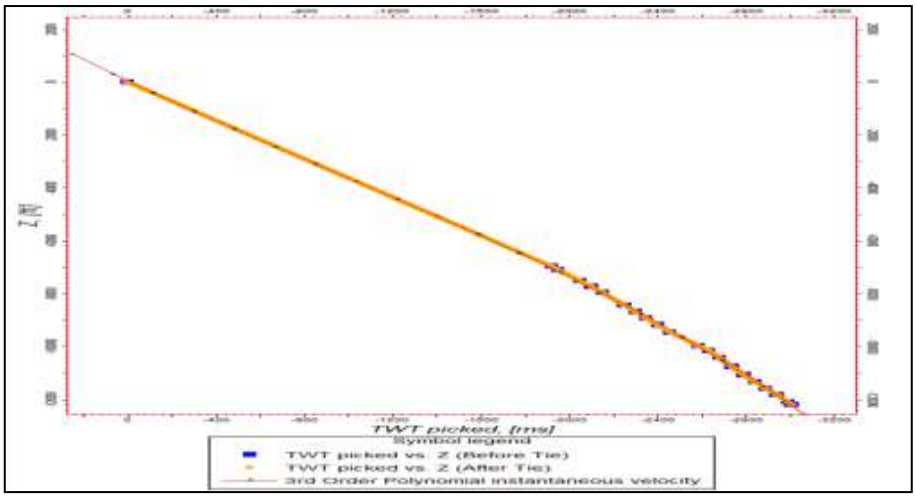


**Figure 9: Third Order Polynomial Velocity Model Utilized for Converting Reservoir Surfaces from Time to Depth**

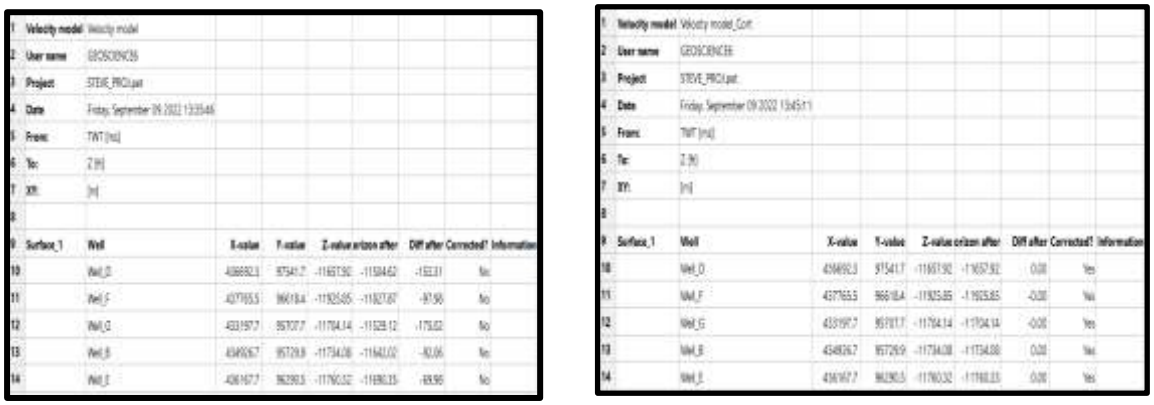

(a) (b)

**Figure 10: Velocity Model (a) and (b)**

### 4.4.8 Seismic Attribute Analysis

Variance attributes were used to map the structure and shape of geological features of interest, such as faults, subtle faults, anticlines, channels and fractures.

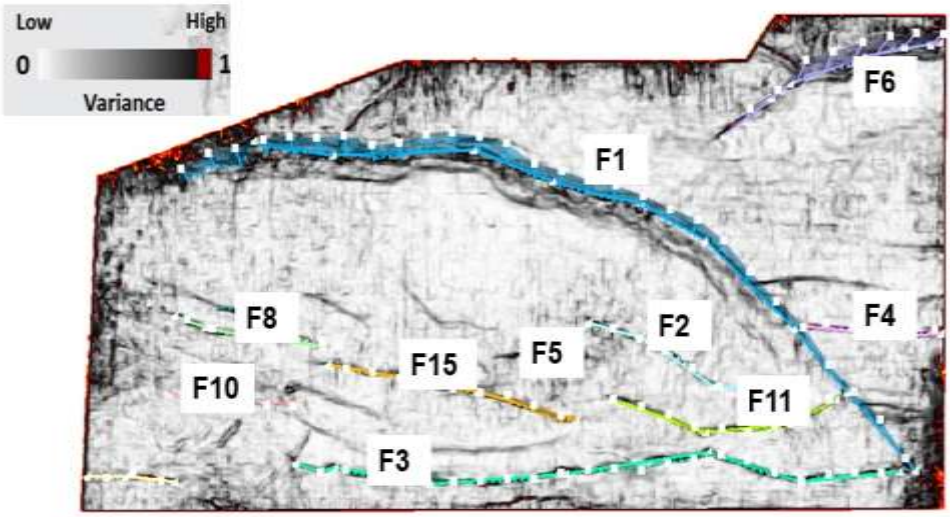


**Figure 11: Variance attributes (at 2000 seconds) to delineate major faults and minor faults**

**4.4.9 Fault interpretation**

The faults were initially identified on the time slices using the variance property, then on the inline direction. This was required to ascertain the horizontal extent of the fault traces. The inline direction was chosen because it is perpendicular to the geologic strike and structures are found in this direction.

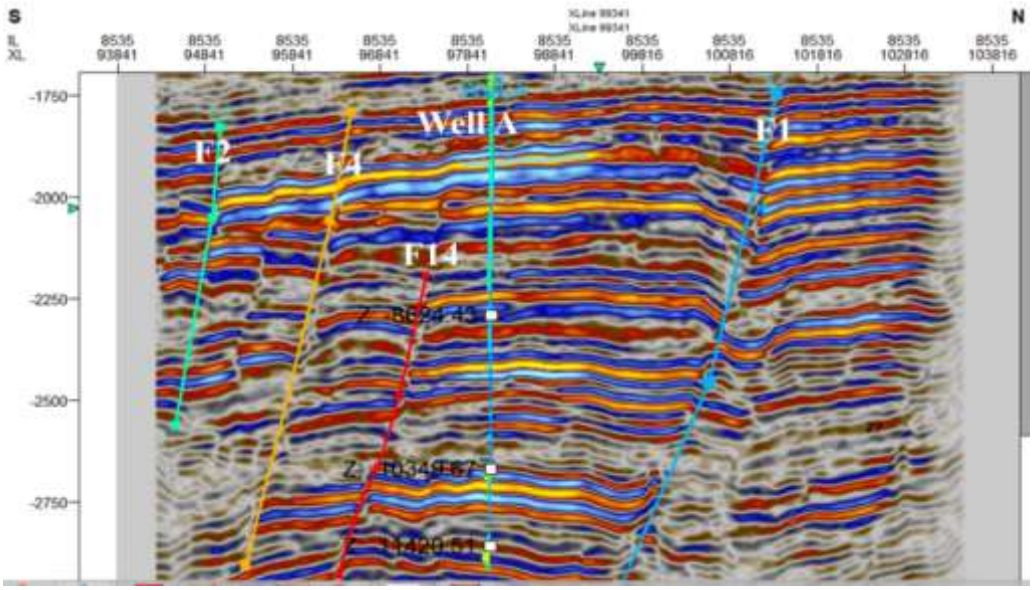


**Figure 12: Seismic inline 8535 showing interpreted synthetic and antithetic faults**

**4.4.10 Structural Smoothing:**

Structural smoothing was carried out on the seismic data to enhance the visibility of geological structures and reduced noise. This is shown in Figure 13 – Figure 15

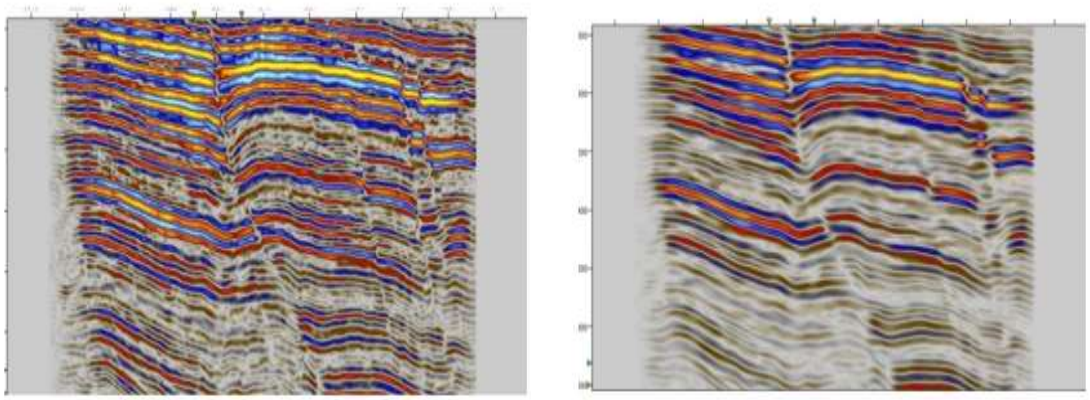

(a) Raw Seismic Data without applying Structural Smoothing.

(b) Raw Seismic Data with a Structural Smoothing.

**Figure 13: Effect of structural smoothing (a) Raw Seismic Data without Applying Structural Smoothing) and (b) the Application of Structural Smoothing**

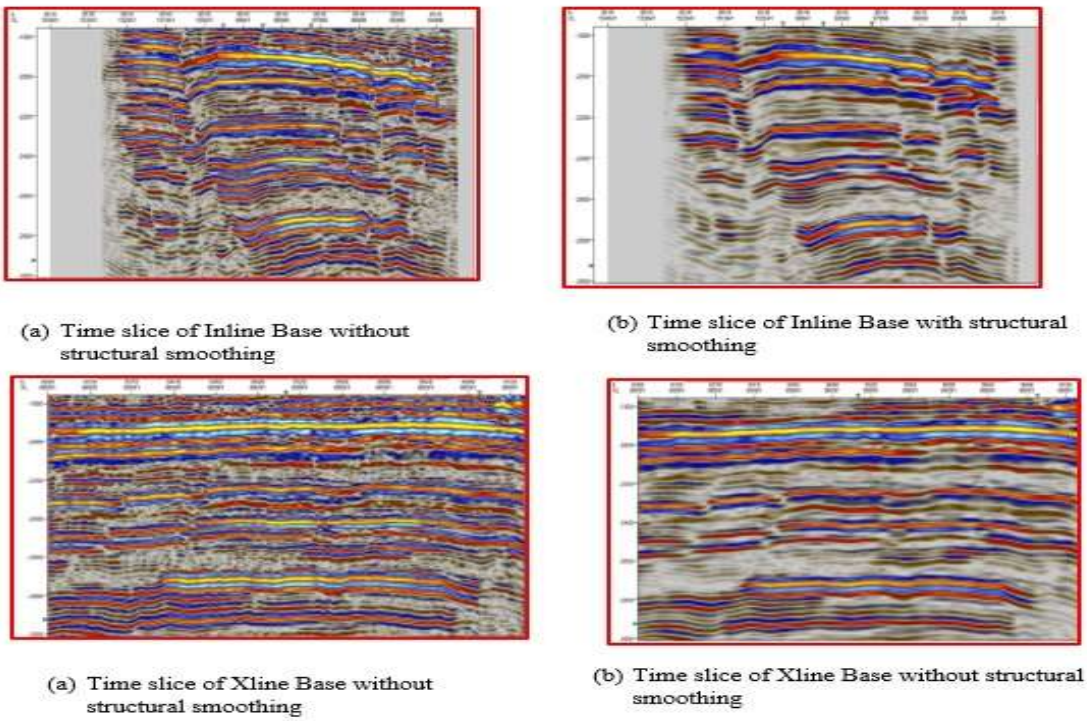

(a) Time slice of Inline Base without structural smoothing

(b) Time slice of Inline Base with structural smoothing

(a) Time slice of Xline Base without structural smoothing

(b) Time slice of Xline Base without structural smoothing

**Figure 14: Shows Time Slice of Inline and Xline of the Seismic Data for both Base and Monitor without Structural Smoothing and the Application of Structural Smoothing Respectively.**

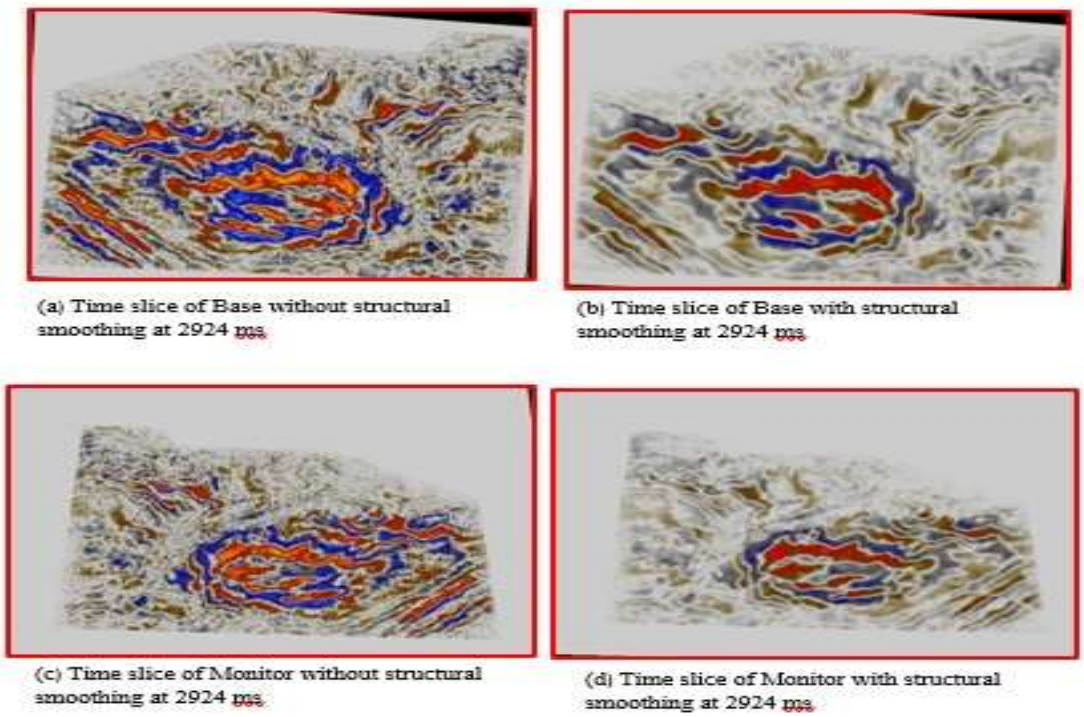


**Figure 15: Time Axis of the Seismic Data for both Base and Monitor without Structural Smoothing and the Application of Structural Smoothing Respectively.**

### 4.4.11 Ant-Attributes

The Subtle faults delineation from Ant Attributes

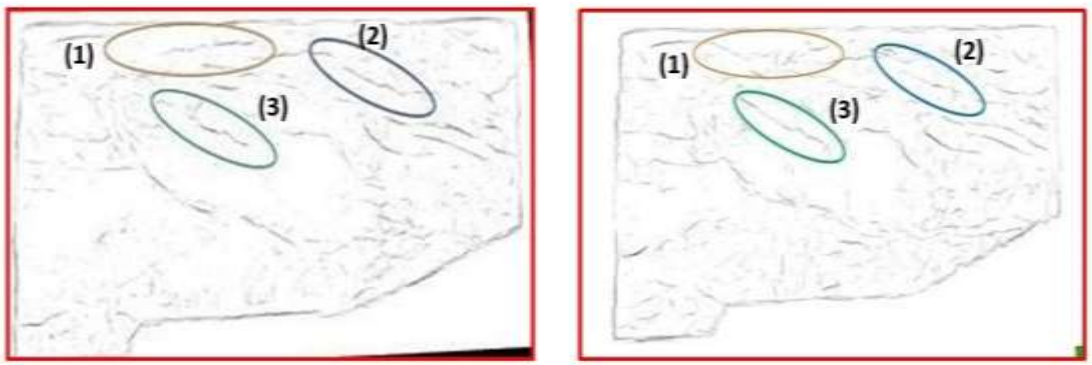


**(a) Base Map** **(b) Monitor Map**

**Figure 16: Shows Ant attributes at 2248 seconds for both base and monitor delineating subtle faults respectively.**

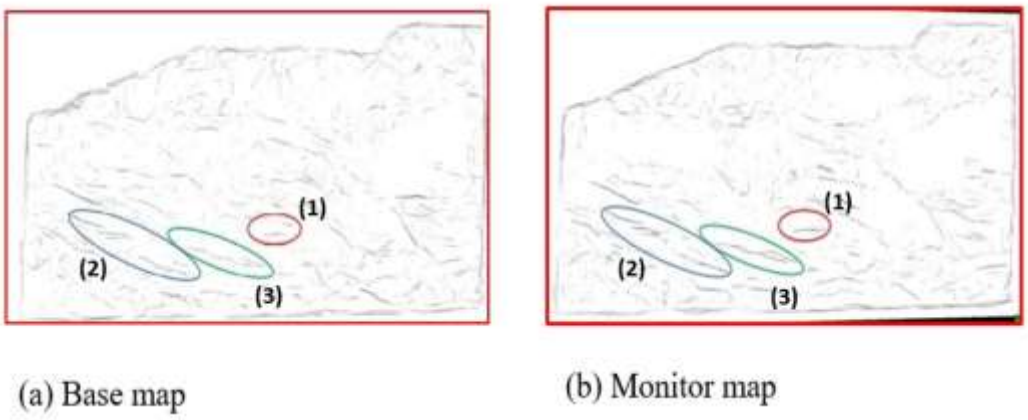


**Figure 17: Ant attribute at 2536 seconds for both base and monitor delineating subtle faults**

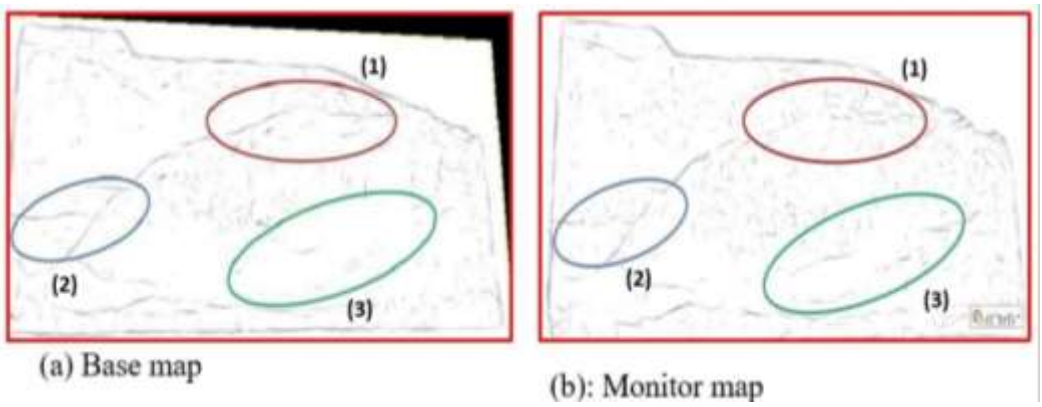


**Figure 18: Shows Ant attribute at 2000 seconds for both base and monitor delineating subtle faults respectively.**

In this study, the seismic data used was carefully conditioned using structural smoothing to remove residual background noise and to improve the spatial continuity of seismic signal (Figures 13-15). Then, variance attributes (Figure 11) which is sensitive to faults was applied to the seismic data set; and the outputs from these processes was used as our input data to run the ant attribute (Figures 16 -18) with which the faults were clearly seen that were difficult to display on the raw seismic data set. The results obtained from the ant attribute monitor volume indicate that the subtle faults seen in the base volume are fractured, reactivated in the monitor volume due to fluid production. The Ant Tracker Attribute indeed enhances faults and fractures in 3D data set

**4.5 Determination of Acoustic Impedance from Monitor Seismic Data**

Acoustic impedance is used to understand the subsurface geology and identifying potential reservoirs. Also, to predict rock properties, such as porosity and fluid saturation. The changes in acoustic impedance were used to indicate changes in rock properties or lithology as a result of hydrocarbon production induced stress change. Figure 20 shows acoustic impedance maps for SAND 2. There is a low acoustic impedance in the base map indicating hydrocarbon zone. As production continuous a reduction in Shear Strength of the rocks surrounding the reservoir in the monitor vintage was observed resulting to fracture.

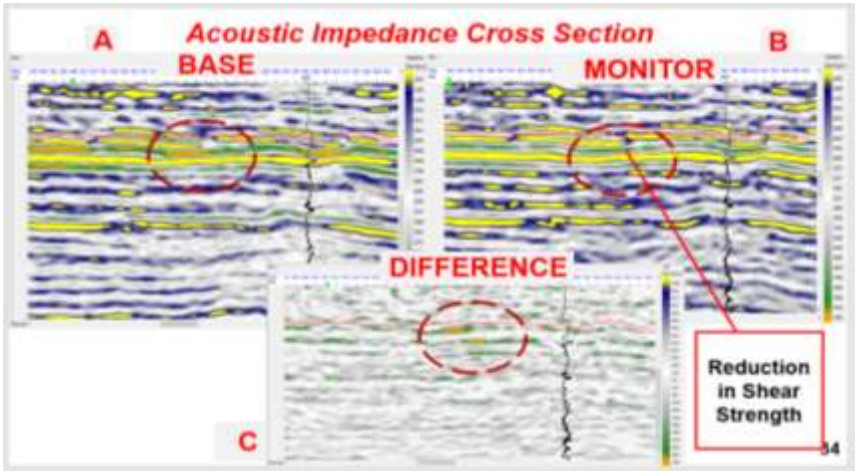


**Figure 19: Acoustic impedance slice for(A) Base (B) Monitor and (C) difference volume**

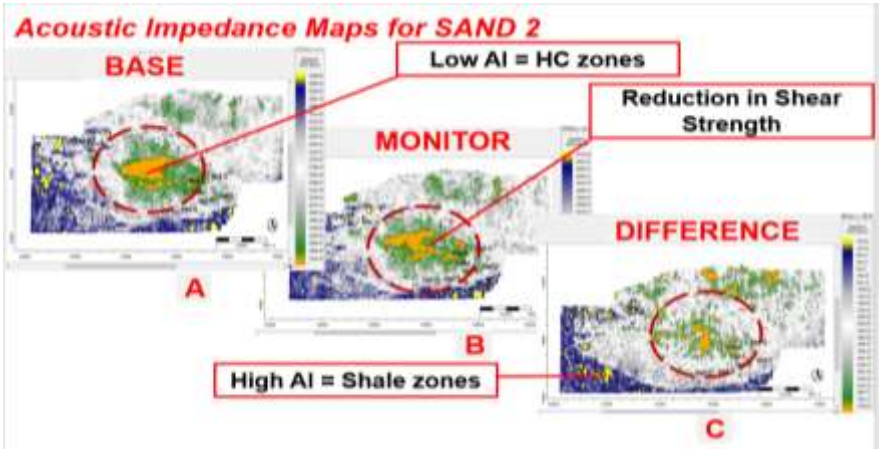


**Figure 20: Acoustic Impedance Map for (A) Base (B) Monitor and (C) difference volume**

### 4.6 Determination of Effective Pressure

The Eaton method was used to estimates pore pressure from the ratio of acoustic travel time (Δt) in normally compacted sediments to the observed acoustic travel time. The result reveals a reduction in pressure in the monitor vintage due to fluid production.

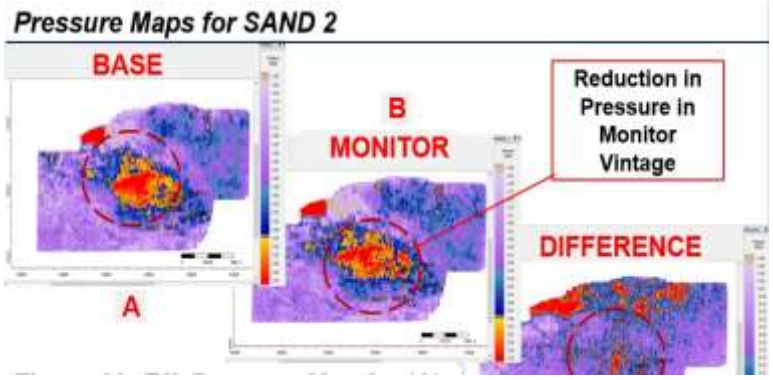


**Figure 21: Effective Pressure Map for (A) Base (B) Monitor and (C) difference volume**

**4.7 Production and Pressure Data**

The Production data and Pressure data were obtained from Shell Petroleum Development Company (SPDC), Port Harcourt Office as shown in Table 6. Production and pressure data is a routine dynamic monitoring of reservoir development. The data were used to monitor mostly fluid production flow rates of individual wells and the effect on pressure; the reservoir's overall flow rate and the cumulative production of each fluid produced from the reservoir over time and its effects on pressure. The gas-oil ratio and water cut were also monitored.

In Table 7, pressure decline was observed as Oil production days increases.

The result obtained from well C and Well D shows pressure and oil production rate decline, as oil production days and wat cut increases. This could be as a result of loss of porosity and permeability or rock displacement and fractured caused by overburden pressure from overlying rocks, which validates the induced-stress change in the reservoir rock due to fluid production.

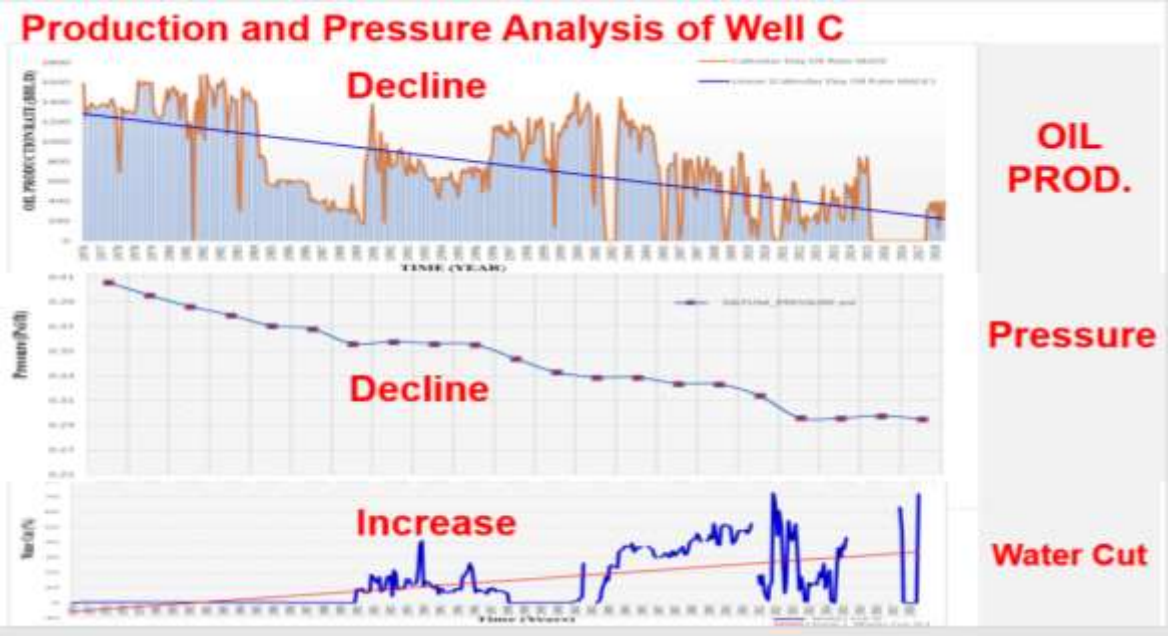


**Figure 22: Production and Pressure Analysis of Well C**

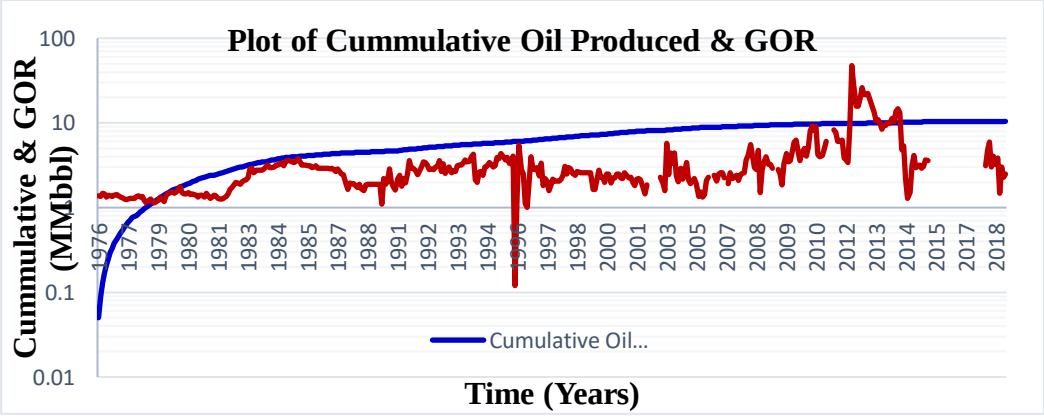


**Figure 23: Cumulative & GOR (MMbbl) for Well C between 1979 to 2018**

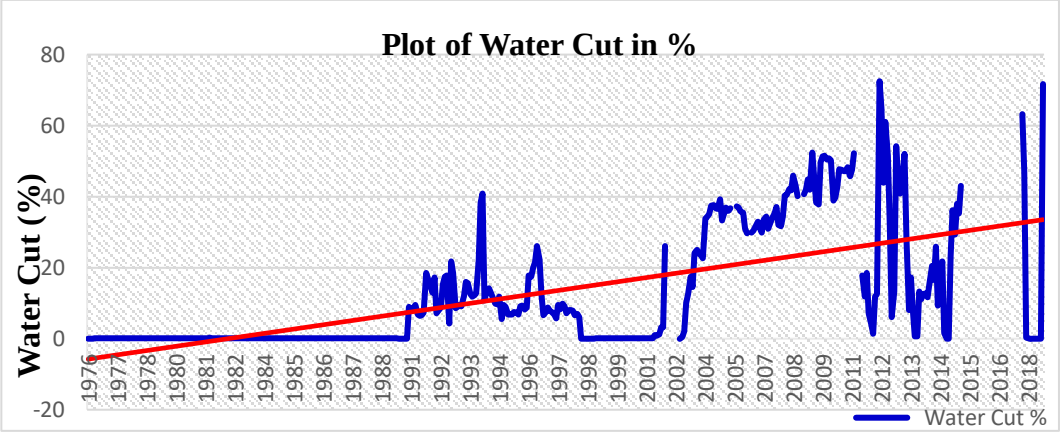


**Figure 24: Plot of Water Cut in % in Well C**

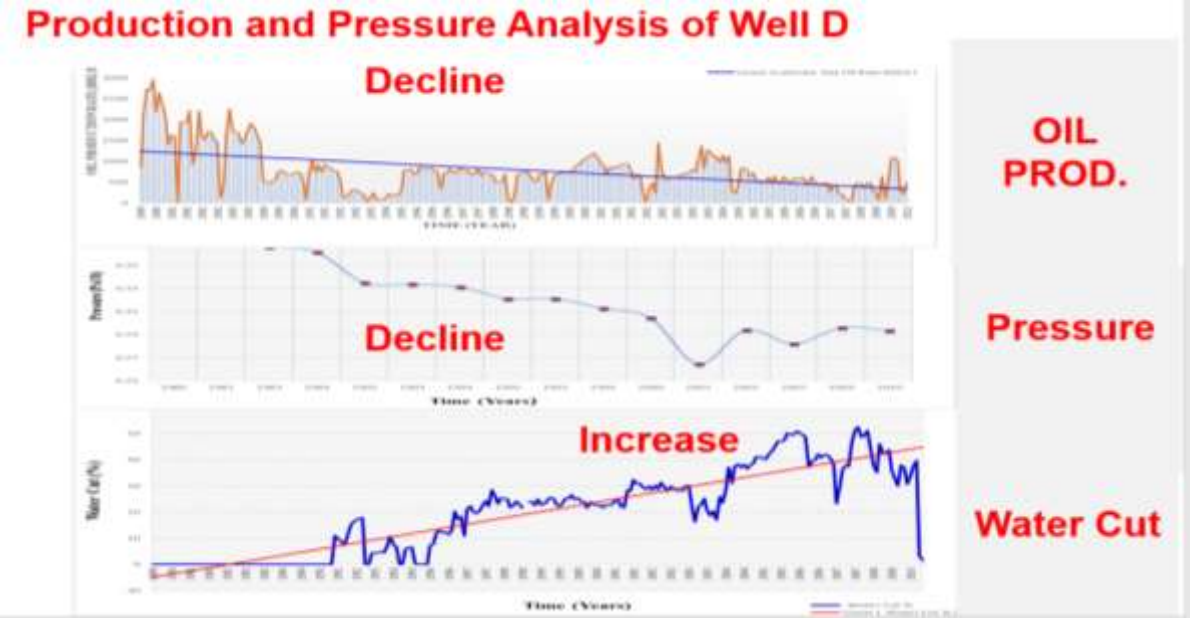


**Figure 25: Production and Pressure Analysis of Well D**

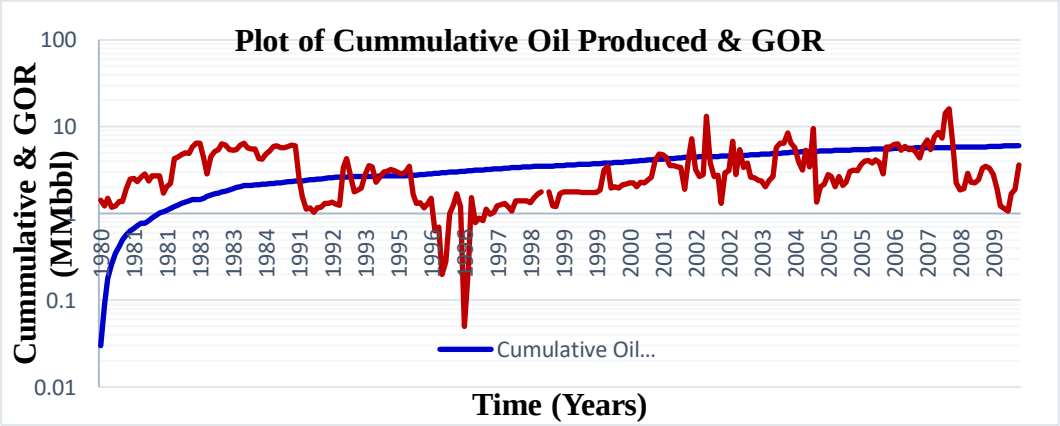


**Figure 26: Plot of Water Cut in % in Well D**

**Table 6: Kolo-Creek Field Reservoir Pressure History**

| DAYS Oil Production (Days) | Reservoir Pressure (psi) |
|---|---|
| 1 | 4766 |
| 603 | 4645 |
| 974 | 4538 |
| 1372 | 4456 |
| 1988 | 4355 |
| 2631 | 4325 |
| 3921 | 4184 |
| 4016 | 4201 |
| 4324 | 4184 |
| 4709 | 4175 |
| 5991 | 4043 |
| 6652 | 3914 |
| 6924 | 3864 |
| 7256 | 3804 |
| 7502 | 3798 |
| 8100 | 3690 |
| 12872 | 3478 |
| 13312 | 3474 |
| 13884 | 3498 |
| 14576 | 3467 |

**Table 7: Kolo-Creek Field Oil Production Rate for Well C**

| Days | Calendar Day Oil Rate (bbl/d) |
|---|---|
| 1 | 1592.55 |
| 30 | 1254.68 |
| 60 | 1348.97 |
| 90 | 1334.00 |
| 120 | 1389.77 |
| 150 | 1378.35 |
| 180 | 1346.58 |
| 210 | 1354.18 |
| 240 | 1349.00 |
| 270 | 1366.33 |
| 300 | 1386.00 |
| 330 | 1375.47 |
| 360 | 1371.81 |
| 390 | 1347.81 |
| 420 | 1402.00 |
| 450 | 1437.94 |
| 480 | 1385.70 |
| 510 | 1345.68 |
| 540 | 970.84 |
| 570 | 695.68 |
| 600 | 1347.65 |

| | |
|---|---|
| 630 | 1330.37 |
| 660 | 1284.00 |
| 690 | 1304.30 |
| 720 | 1317.42 |
| 750 | 1300.81 |
| 780 | 1284.83 |
| 810 | 1288.58 |
| 840 | 1370.20 |
| 870 | 1624.35 |
| 900 | 1562.71 |
| 930 | 1578.71 |
| 960 | 1610.71 |
| 990 | 1578.93 |
| 1020 | 1595.29 |
| 1050 | 1601.47 |
| 1080 | 1599.32 |
| 1110 | 1351.03 |
| 1140 | 1283.37 |
| 1170 | 1244.10 |
| 1200 | 1230.70 |
| 1230 | 1235.58 |
| 1260 | 1268.16 |

## 5. CONCLUSION

Hydrocarbon Production induced-stress change in Reservoirs have been successfully carried out using seismic data and well log data in Kolo-Creek Oil Field in the Coastal Swamp Niger Delta, Nigeria to evaluate production induced-stress on a producing reservoir. Three zones of interest (Sand A, Sand B and Sand C) were delineated and correlated across all seven wells. The litho-stratigraphy correlation section revealed that each of the sand units spreads over the field and differs in thickness with some units occurring at greater depth than their adjacent unit that is possibly evidence of faulting. The petrophysical parameters calculated include total/effective porosity, water/hydrocarbon saturation, permeability, net-to-gross and volume of shale. Also, seismic attributes like coherence variance and ant tracker attributes were interpreted

The Days of Oil Production data versus Reservoir Pressure data were obtained from Shell Petroleum Development Company (SPDC), Port Harcourt Office as shows a pressure decline and oil production rate as oil production days increases. This could be as a result of loss of porosity and permeability or rock displacement and fractured caused by overburden pressure from overlying rocks, which validates the induced-stress change in the reservoir rock as a production effect. The ant tracker attributes reveals that the subtle faults seen in the base volume are fractured, some fault re-activated in the monitor volume resulting to pressure depletion, loss of porosity, permeability and change in stress and strain in the overburden reservoir. The results of this work can be used as a tool for monitoring oil production pressure and oil production rate per day of a producing reservoir life. This study also has proven that the evaluating hydrocarbon production induced-stress change in a reservoir is key factor for effective productivity of hydrocarbons.

**ACKNOWLEDGEMENT**

The authors are thankful to Nigeria National Petroleum Company (NNPC) for the permission given to us to obtain data from The Shell Petroleum Development Company (SPDC) Nigeria Limited.

**REFERENCES:**


- Abakumov, I., Johann, L., Shapiro, S. A., Pasternak, E., & Dyskin, A. V. (2020). Towards integrated modeling of deformations, time-lapse seismic changes, and failure stresses caused by massive underground fluid operations. *SEG Technical Program Expanded Abstracts 2020*. https://doi.org/10.1190/segam2020-3427353.1
- Adeleye, D. R. (1975). Nigerian Late Cretaceous stratigraphy and paleogeography. *AAPG Bulletin, 59*(12), 2302–2313.
- Aguado, D. B., Kaschaka, A., & Pinheiro, L. F. (2009). *Seismic attributes in hydrocarbon reservoir characterization*. Universidade de Aveiro.
- Aki, K., & Richards, P. G. (1980). *Quantitative seismology*. W. H. Freeman.
- Allan, U. S. (1989). Model for hydrocarbon migration and entrapment within faulted structures. *AAPG Bulletin, 73*, 803–811.
- Allen, D. R., & Mayuga, M. N. (1969). The mechanics of compaction and rebound, Wilmington oilfield, Long Beach, California, USA. In *Land subsidence* (Vol. 89, No. 2, pp. 410–413). IAHS–UNESCO.
- Alsos, T., Eide, A., Astratti, D., Pickering, S., Benabentos, M., Dutta, N., Mallick, S., Schultz, G., Den Boer, L., Livingston, M., Nickel, M., Sonneland, L., Schlaf, J., Schoepfer, P., Sigismondi, M., Soldo, J. C., & Stronen, L. K. (2002). Seismic applications throughout the life of the reservoir. *Oilfield Review, 14*, 48–65.
- Amoyedo, S. O., Marfurt, K. J., & Slatt, R. M. (2012). Time-lapse (4D) seismic effects: Reservoir sensitivity to stress and water saturation. In *SEG Annual Meeting Expanded Abstracts*. Society of Exploration Geophysicists.
- Aniwetalu, E. U., Anakwuba, E. K., Ilechukwu, J. N., & Aikegwuonu, O. N. (2017). Application of time-lapse (4D) seismic data in locating hydrocarbon prospects in Udam Field, onshore Niger Delta, Nigeria. *Petroleum and Coal, 59*(5), 715–722.
- Asseez, L. O. (1976). Review of the stratigraphy, sedimentation and structure of the Niger Delta. In C. A. Kogbe (Ed.), *Geology of Nigeria* (pp. 259–272). Elizabeth Press.
- Barkved, O. I., & Kristiansen, T. (2005). Seismic time-lapse effects and stress changes: Examples from a compacting reservoir. *The Leading Edge, 24*(12), 1244–1248.
- Barkved, O., Heavey, P., Kjelstadli, R., Kleppan, T., & Kristiansen, G. (2003). *Valhall field—Still on plateau after 20 years of production* (SPE Paper 83957). Society of Petroleum Engineers.
- Batzle, M., & Wang, Z. (1992). Seismic properties of pore fluids. *Geophysics, 57*(11), 1396–1408.
- Boutte, D. (2007). *Seismic-to-simulation arrives*. E&P Management Report. Hart Energy Publishing.
- Bruno, M. (2002). Geomechanical and decision analyses for mitigating compaction-related casing damage. *SPE Drilling & Completion, 17*(3), 179–188.
- Buland, A., & Omre, H. (2003). Bayesian linearized AVO inversion. *Geophysics, 68*(1), 185–198.
- Buland, A., & El Ouair, Y. (2006). Bayesian time-lapse inversion. *Geophysics, 71*(3), R43–R48.
- Chin, L. Y., & Nagel, N. B. (2004). Modeling of subsidence and reservoir compaction under waterflood operations. *International Journal of Geomechanics, 4*(1), 28–34.
- Chopra, S., & Marfurt, K. J. (2010). *Seismic attributes for prospect identification and reservoir characterization*. Society of Exploration Geophysicists.
- Colazas, X. C., & Strehle, R. W. (1995). Subsidence in the Wilmington oil field, Long Beach, California, USA. In G. V. Chilingarian et al. (Eds.), *Subsidence due to fluid withdrawal* (pp. 285–336). Elsevier.
- Cole, S., Lumley, D., Meadows, M., & Tura, A. (2002). Pressure and saturation estimation from 4D seismic data by rock physics forward modeling. In *72nd Annual International Meeting, SEG Expanded Abstracts* (pp. 2475–2478).
- Cox, T., & Seitz, K. (2007). Ant tracking seismic volumes for automated fault interpretation. In *CSPG/CSPE GeoConvention Proceedings*. Calgary, Canada.
- Spetzler, J., & Kvam, O. (2006). Discrimination between phase and amplitude attributes in time-lapse seismic streamer data. *Geophysics, 71*(4), I9–I19.

- Stacher, P. (1995). Present understanding of the Niger Delta hydrocarbon habitat. In M. N. Oti & G. Postma (Eds.), *Geology of deltas* (pp. 257–267). A. A. Balkema.
- Staples, R., Cook, A., Braisby, J., Hodgson, B., & Mabillard, A. (2006). Integration of 4D seismic data and the dynamic reservoir model reveal new targets in Gannet C. *The Leading Edge, 25*, 1126–1130.
- Staples, R., Ita, J., Burrell, R., & Nash, R. (2007). Monitoring pressure depletion and improving geomechanical models of the Shearwater Field using 4D seismic. *The Leading Edge, 26*, 636–641.
- Uko, E. D., & Otugo, V. N. (2018). Time-lapse analysis of the effects of oil and gas exploitation using remote sensing and GPS in parts of the Niger Delta, Nigeria. *Journal of Geography, Environment and Earth Science International, 5*(4), 1–13.
- Uko, E. D., Famuyibo, D. A., & Okiongbo, K. (2018). Estimation of land surface subsidence induced by hydrocarbon production in the Niger Delta, Nigeria, using time-lapse orthometric leveling data. *Mediterranean Journal of Basic and Applied Sciences, 2*(3), 1–18.
- Uko, E. D., Ekine, A. S., Ebeniro, J. O., & Ofoegbu, C. O. (1992). Weathering structure of the East Central Niger Delta, Nigeria. *Geophysics, 57*(9), 1228–1233.
- Van der Kooij, M. (1997). *Land subsidence measurements at the Belridge oil fields from ERS InSAR data*. Proceedings of the 3rd ESA ERS Symposium, Florence, Italy. http://earth.esa.int/workshops/ers97/papers/vanderkooij1/index-2.htm
- Varela, O. J., Torres-Verdín, C., Sen, M. K., & Roy, I. G. (2006). Using time-lapse seismic amplitude data to detect variations of pore pressure and fluid saturation due to oil displacement by water: A numerical study based on one-dimensional prestack inversion. *Journal of Geophysics and Engineering, 3*(2), 177–193.
- Vedanti, N., Pathak, A., Srivastava, R. P., & Dimri, V. P. (2009). Time-lapse (4D) seismic: Some case studies. *e-Journal Earth Science India, 2*(4), 230–248.
- Veeken, P. C. H., & Da Silva, M. (2004). Seismic methods and some of their constraints. *First Break, 22*(1), 47–70.
- Wang, Z. (2001). Fundamentals of seismic rock physics. *Geophysics, 66*(2), 398–412.
- Weber, K. J., & Daukoru, E. M. (1975). Petroleum geology of the Niger Delta. In *9th World Petroleum Congress Proceedings* (Vol. 2, pp. 209–222).
- White, W. A., & Morton, R. A. (1997). Wetland losses related to fault movement and hydrocarbon production, southeastern Texas coast. *Journal of Coastal Research, 13*, 1305–1320.
- White, W. A., & Tremblay, T. A. (1995). Submergence of wetlands as a result of human-induced subsidence and faulting along the upper Texas Gulf Coast. *Journal of Coastal Research, 11*, 788–807.
- Wyllie, M. R. J., Gregory, A. R., & Gardner, G. H. F. (1958). An experimental investigation of factors affecting elastic wave velocities in porous media. *Geophysics, 23*(3), 459–493.
- Zoback, M. D., & Zinke, J. C. (2002). Production-induced normal faulting in the Valhall and Ekofisk oil fields. *Pure and Applied Geophysics, 159*(1–3), 403–420.
- Zoback, M. D., Chan, A. W., & Zinke, J. (2002). Production-induced normal faulting. In *Proceedings of the 38th U.S. Rock Mechanics Symposium (DC Rocks 2001)* (pp. 157–163). Washington, DC.